Journal Name

ARTICLE

A robust solid oxide electrolyzer for highly efficient electrochemical reforming of methane and steam

Received 00th January 20xx,
Accepted 00th January 20xx

DOI: 10.1039/x0xx00000x

www.rsc.org/

Tong Liu,[*ab] Hao Liu,[a] Xiaoyu Zhang,[a] Libin Lei,[c] Yanxiang Zhang,[d] Zhihao Yuan,[e] Fanglin Chen,[c] and Yao Wang[*ab]

In this work, a robust solid oxide electrolysis cell with $Sr_2Fe_{1.5}Mo_{0.5}O_{6-\delta}$-$Ce_{0.8}Sm_{0.2}O_{1.9}$ (SFM-SDC) based electrodes has been utilized to verify the conceptual process of partial oxidation of methane (POM) assisted steam electrolysis, which can produce syngas and hydrogen simultaneously. When the cathode is fed with 74%H_2-26%H_2O and operated at 850 °C, the open circuit voltage (OCV), the minimum energy barrier required to overcome the oxygen partial gradient, is remarkably reduced from 0.940 to -0.012 V after shifting the feeding gas in the anode chamber from air to methane, indicating that the electrical consumption of steam electrolysis process could be significantly reduced and compensated by the use of low grade thermal energy from external heat sources. It is found that after ruthenium (Ru) impregnation, the electrolysis current density of the electrolyzer is effectively enhanced from -0.54 to -1.06 Acm^{-2} at 0.6 V and 850 °C, while the electrode polarization resistance at OCV condition and 850 °C is significantly decreased from 0.516 to 0.367 Ωcm^2. Long-term durability testing demonstrates that no obvious degradation but a slight improvement is observed for the electrolyzer, which is possibly due to the activation of the SFM-SDC electrode during operation. These results indicate that the robust Ru infiltrated solid oxide electrolyzer is a very promising candidate for POM assisted steam electrolysis application. Our result will provide insight to improve the electrode catalysts used in POM assisted steam electrolysis.

1. Introduction

Hydrogen (H_2) has been considered as one of the leading energy carrier candidates for the future because it has the highest energy content by fuel weight and can be produced from a wide variety of energy sources[1-4], such as natural gas, biomass and discarded oil. Currently, most hydrogen is produced by steam methane reforming (SMR) process[5-7], but it suffers from several drawbacks, such as the emission of greenhouse gas (CO_2) and the high capital cost. Steam electrolysis is an alternative method to alleviate these drawbacks because this technology can directly convert water/steam to pure hydrogen and oxygen without the release of CO_2[8-16], but hydrogen generated by steam electrolysis process is at least two to three times more expensive than that produced by SMR process due to the high consumption of electricity, which is an expensive form of energy. Fortunately, the energy required for steam electrolysis process can be supplied in a mixed form of electricity and heat[8,17]. According to the thermodynamics of steam splitting reaction, the proportion of electrical energy demand to the total energy demand has effectively decreased with increasing the operating temperature, indicating that certain amount of expensive electrical energy could be compensated by the use of low grade cheap thermal energy from external heat sources. Therefore, steam electrolysis via a solid oxide electrolysis cell (SOEC) operated at elevated temperature (600-1000 °C) has been demonstrated to be a more efficient method to produce hydrogen[8-16]. However, due to the expensive electricity cost, more than two thirds of the total hydrogen production cost are still attributed to the electricity. Therefore, the electricity consumption of the electrolyzer must be further reduced to make high temperature steam electrolysis process competitive to conventional SMR process[8,17,18]. Recently, some reducing substances such as methane (CH_4), carbon (C), carbon monoxide (CO), natural gas and H_2 instead of air have been fed into the anode side to further assist steam electrolysis process[17,19-27], and it has been demonstrated that the electrical consumption is significantly reduced while the energy efficiency is strongly enhanced. In this fuel assisted mode, the anode and cathode are both exposed to a reducing atmosphere and the oxygen partial pressure gradient across the electrolyte could be significantly reduced, substantially decreasing the open circuit voltage (OCV) to (near) zero or even a negative value. As a result, oxygen ions (O^{2-}) can be more easily and effectively

[a] Key Laboratory of Hydraulic Machinery Transients (Wuhan University), Ministry of Education, School of Power and Mechanical Engineering, Wuhan University, Wuhan, Hubei 430072, China
[b] Suzhou Institute of Wuhan University, Suzhou, Jiangsu 215123, China
[c] Department of Mechanical Engineering, University of South Carolina, Columbia, SC 29208, USA
[d] National Key Laboratory for Precision Hot Processing of Metals, School of Materials Science and Engineering, Harbin Institute of Technology, Harbin, Heilongjiang 150001, China
[e] School of Materials Science and Engineering, Tianjin University of Technology, Tianjin 300384, China
* Email: liu_tong@whu.edu.cn (T. Liu), pmewy@whu.edu.cn (Y. Wang)
† Footnotes relating to the title and/or authors should appear here.
Electronic Supplementary Information (ESI) available: [Raman spectra for SFM powders, and *i-V* curves of solid oxide electrolyzers for steam electrolysis in conventional mode and POM assisted mode.]. See DOI: 10.1039/x0xx00000x

pumped from the cathode chamber to the anode chamber. Our previous work has evaluated the thermodynamics of methane assisted steam electrolysis reaction, the electrical energy, ΔG, required to electrolyze water is replaced by the chemical energy stored in methane, and ΔG is remarkably decreased to 5 kJmol^{-1} at 650 C, which indicates that about 50% of the total energy could be provided by low grade waste heat instead of electricity[17].

Several solid oxide electrolyzers with different electrodes have been developed to perform methane assisted steam electrolysis process[17,22-26]. Wang *et al.* have infiltrated Cu-CeO_2, Co-CeO_2 and Pd-C-CeO_2 into yttria-stabilized zirconia (YSZ) backbone to fabricate Cu-CeO_2-YSZ, Co-CeO_2-YSZ, and Pd-C-CeO_2-YSZ cells[26], and found that OCVs for these cells were much higher than the theoretical value calculated. The discrepancy between experimental and calculated values was possibly attributed to the slow kinetics of methane oxidation, which is limited by the relatively low catalytic activity of the electrodes. As a result, electrodes with higher catalytic activity are required to promote methane assisted steam electrolysis reaction for hydrogen production. In our previous study, $Sr_2Fe_{1.5}Mo_{0.5}O_{6-\delta}$-$Ce_{0.8}Sm_{0.2}O_{1.9}$ (SFM-SDC) cells with Ni infiltration were utilized to verify the concept of methane assisted steam electrolysis process[27], and it is demonstrated that to obtain the same electrolysis current density, the applied voltage in the methane assisted mode can be readily reduced by nearly one order of magnitude when compared with that in the conventional mode. However, it is still a huge waste and environmental unfriendly to use precious CH_4 fuel to assisted steam electrolysis via complete combustion of CH_4 to CO_2 and H_2O[28,29]. Presently, partial oxidation of methane (POM, $CH_4+0.5O_2=CO+2H_2$) to more valuable chemical syngas ($CO+H_2$ mixture) is therefore a technology capable of contributing to a carbon-neutral energy system in the future, and has been considered as one economically available route for the conversion of methane. Therefore, a novel conceptual POM assisted steam electrolysis as schematically shown in Figure 1 is proposed. In this concept, the cathode and anode are exposed to H_2-H_2O mixture and methane, respectively, which can be simultaneously converted to hydrogen and syngas during the operation. Moreover, the pure hydrogen produced in the cathode can be directly used as the fuel, while the products of syngas in the cathode is a high quality feedstock for Fischer-Tropsch (F-T) synthesis. It is well known that the conversion of methane into value-added products via POM process is a challenging task because of the high CH_3-H (g) bond dissociation energy of 439.3 kJ mol^{-1}.[28,29] Heterogeneous catalyst has therefore been a key to the successful conversion of methane to syngas via the POM process, and the reason is that the bond dissociation energy of CH_x-H depends on the surface of the hosting metal[30-35]. In recent year, ruthenium (Ru), the cheapest among the noble metals, has been widely used for POM reaction because of its high activity, good long-term stability and excellent H_2 and CO selectivity[30,35-38]. Moreover, ion-impregnation is a common and efficient way to fabricate nanostructured electrode with enlarged active reaction sites and good stability[33-35,39-42]. Therefore, in this work, Ru-based nano-electrode prepared via an ion-impregnation method is investigated as a potential candidate toward this novel concept.

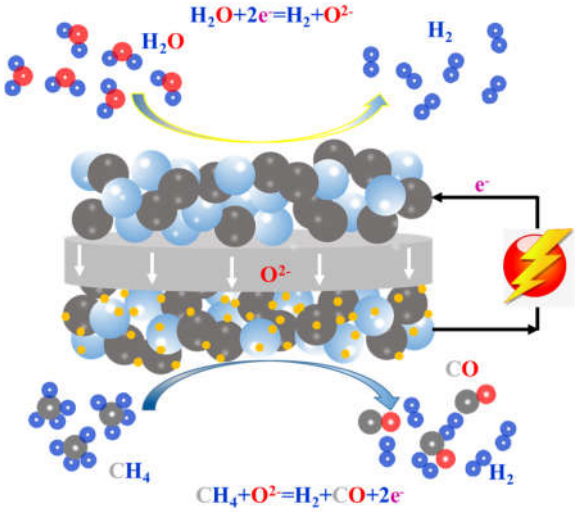

Figure 1 Schematic illustration presenting the concept of methane assisted steam electrolysis.

In this work, Ru-based nanocatalysts are infiltrated to the SFM-SDC skeleton to prepare Ru infiltrated SFM-SDC (Ru-SFM-SDC) nano-electrode via an ion impregnation process, aiming to effectively enhance its catalytic properties for POM process. The outlet gas composition in the anode is determined by using gas chromatography (GC) to validate the concept of POM assisted steam electrolysis. Electrochemical performance is evaluated by using the current density-cell voltage (*i-V*) and impedance spectra measurements. The impedance spectra are further analyzed by distribution relaxation of time (DRT) technique. Long-term stability of solid oxide electrolyzer using Ru infiltrated SFM-SDC electrode as the anode is also investigated.

2. Experimental

2.1 Fabrication of single cells

$La_{0.80}Sr_{0.20}Ga_{0.80}Mg_{0.20}O_{3-X}$ (LSGM)-electrolyte supported single cells with a configuration of Ru-SFM-SDC/LSGM/SFM-SDC were fabricated for POM assisted steam electrolysis process. The LSGM powders were purchased from Fuelcellmaterials Inc. The SFM and SDC powders were synthesized using the citric-assisted combustion method[17,43]. Dense LSGM electrolyte were fabricated by pressing the LSGM powders to pellets and sintering at 1400 °C for 5 hours. SFM-SDC ink with a weight ratio of 50:50 was screen-printed on both sides of the electrolyte and then sintering at 1050 °C for 2 hours to form porous electrode skeleton. Ru catalysts were introduced by drop-depositing $RuCl_3$ solution to the SFM-SDC anode skeleton, which was subsequently dried and fired at 600 °C, and the solid loading of Ru nanoparticles is measured to be 1.5 wt.% by using an electric balance. The effective cell area was 0.88 cm^2.

2.2 Characterization

Raman spectra of the SFM-SDC based electrode before and after infiltration were measured using a confocal Raman microspectroscopy (Renishaw RM-1000). SFM-SDC as well as Ru-SFM-SDC samples were analyzed by X-ray photoelectron spectroscopy (XPS, ESCALAB250Xi) to determine Ru 3p binding energy. The cross-sectional morphologies of the cells as well as the composition of the electrodes were examined using a scanning electron microscope (SEM, Zeiss Ultra Plus FESEM).

Cell tests were performed at a home-made setup, and the details were described in our previous work[19]. During the measurement, the gas compositions in both the anode and cathode chambers can be precisely controlled. Mass flow rate of CH_4, H_2 and N_2 gases was controlled by using digital mass flow controllers (APEX, Alicat Scientific), while water vapor was added precisely to the cathode gas stream via a humidifier by heating liquid water to a certain temperature and then measured using a humidity sensor (HMT 337, Vaisala). In the Ru-SFM-SDC anode side, a total 50 SCCM methane mixture composed of 3 SCCM CH_4 and 47 SCCM N_2 were fed to a humidifier at room temperature, creating a methane atmosphere of 5.8%CH_4-91.2%N_2-3%H_2O, while in the SFM-SDC cathode side, 50 SCCM H_2 were injected to a humidifier, which was heated to generate a water partial pressure of 7497 Pa, creating a gas mixture of 74%H_2-26%H_2O. Electrochemical characterizations including current density-cell voltage (*i-V*) and electrochemical impedance spectra (EIS) measurements were conducted using an electrochemical workstation (Versa STAT 3, Princeton Applied Research). The *i-V* curves were recorded from open circuit voltage (OCV) to 1.0 V with a voltage sweeping speed of 0.03 Vs^{-1}, and EIS under the OCV condition were measured with the voltage amplitude of 30 mV in the frequency range from 10^6 to 10^{-2} Hz. The components of the outlet gas in the anode side were analyzed by using a gas chromatograph (GC, Agilent 7890A) while the steam content was determined by using a humidity sensor (HMT 337, Vaisala). The CH_4 conversion (X_{CH4}), CO selectivity (S_{CO}) and H_2 selectivity (S_{H2}) in the anode side are calculated by using the following equations:

$$X_{CH_4} = \frac{F_{in,\,CH_4} - F_{out,\,CH_4}}{F_{in,\,CH_4}} \times 100\%$$

$$S_{CO} = \frac{F_{out,\,CO}}{F_{in,\,CH_4} - F_{out,\,CH_4}} \times 100\%$$

$$S_{H_2} = \frac{F_{out,H_2}}{\left(F_{in,\,CH_4} - F_{out,\,CH_4}\right) \times 2 + F_{in,\,H_2O} - F_{out,\,H_2O}} \times 100\%$$

3. Results and discussion

3.1 Morphology and phase composition of the electrolyzer

Figure 2A shows the cross-sectional SEM image of the solid oxide electrolyzer for POM assisted steam electrolysis process. It is shown that the LSGM electrolyte is about 500 µm thick, and the thickness of the electrode is about 30 µm. During the operation of steam electrolysis process, when the cathode and the anode are exposed to 74%H_2O-26% H_2 and air, respectively, an OCV of 0.940 V at 850 °C is achieved for the cells, which is very close to the theoretical value calculated by Nernst equation, indicating that the electrolyte is dense enough for steam electrolysis application. Meanwhile, as shown in Figure 2B, the SFM-SDC electrodes are porous and well-attached to the dense LSGM electrolyte. After the introduction of $RuCl_3$ solution to the skeleton and heat-treatment at 600 °C for 2h, spheroidal nanoparticles with an average diameter of 100 nm are observed and uniformly distributed on the SFM-SDC skeleton (Figure 2C), forming the Ru-SFM-SDC electrode and serving as the anode for POM reaction.

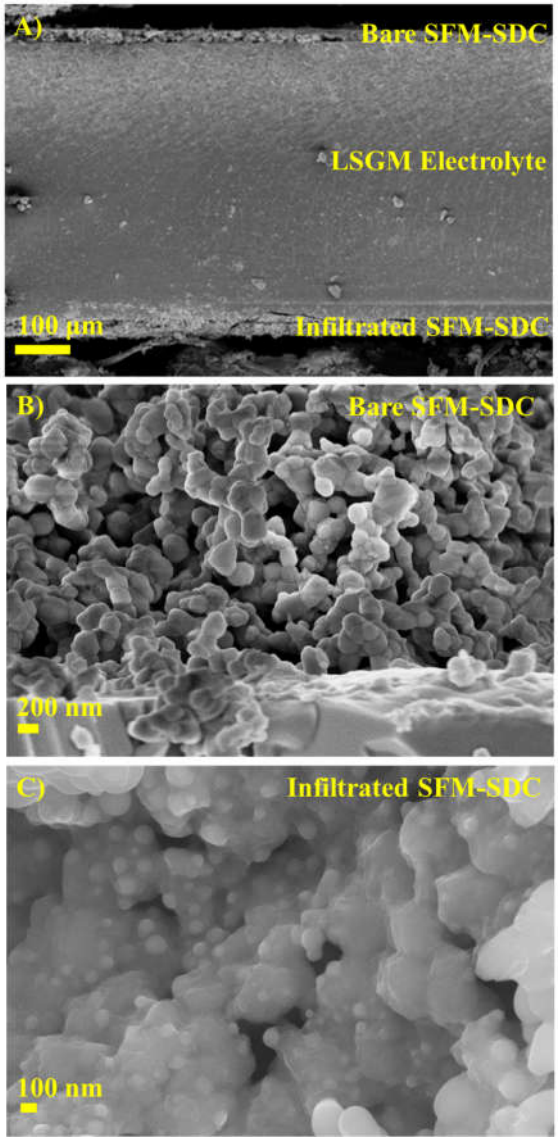

Figure 2 Cross-sectional SEM images of A) Ru-SFM-SDC/LSGM/SFM-SDC cell, B) SFM-SDC cathode/LSGM electrolyte interface, and C) infiltrated SFM-SDC anode.

To further confirm that Ru nanocatalysts have been successfully introduced into the SFM-SDC skeleton, Raman scattering analysis and XPS analysis have also been utilized to determine the phase compositions of the Ru-SFM-SDC electrode. The Raman spectra for the SFM-SDC anode with and without infiltration are shown in Figure 3A. As shown in the Raman spectrum for the bare SFM-SDC anode (Figure 3A), three typical active modes in the range of the experimentals (300-1000 cm^{-1}) are observed in the vicinity of the single crystal signal positions

(459, 554, and 821 cm^{-1}). The former two active modes are in consistent with the SDC signature reported previously[44], while the latter one fits well to the results for SFM powders (Figure S1). After infiltration of $RuCl_3$ solution to the skeleton and heat-treatment in air, a new active mode is clearly observed for the Ru-SFM-SDC anode in the range of 650-750 cm^{-1}, which is assigned to be RuO_2[45]. Figure 3B shows the XPS spectrum of Ru 3p for the bare SFM-SDC anode and Ru infiltrated SFM-SDC anode. The peak at 486 eV associated to the typical binding energy for Ru 3p is only observable in the Ru-SFM-SDC anode, indicating that Ru element presents in the Ru-SFM-SDC sample. These results indicate that Ru element in the form of RuO_2 has been successfully introduced into the SFM-SDC skeleton. During the performance test, RuO_2 nanoparticles can be reduced to Ru nanoparticles by the reducing atmosphere such as CH_4[46], which can serve as the active catalyst for the POM reaction.

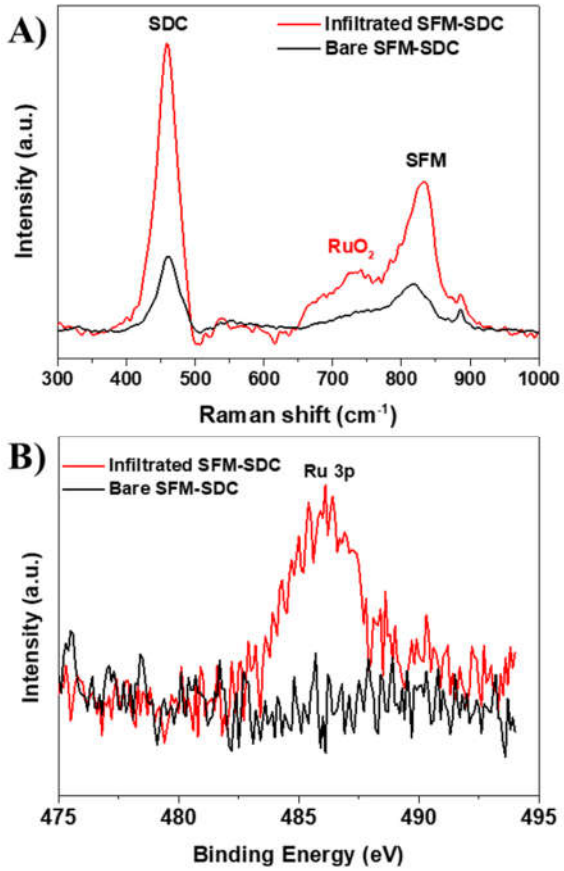

Figure 3 A) Raman spectra, and B) XPS core-level Ru 3p spectra for bare SFM-SDC electrode (black line) and infiltrated SFM-SDC electrode (red line).

3.2 Electrical properties

Single cells using Ru infiltrated SFM-SDC composite as the anode for POM assisted steam electrolysis process are electrochemically characterized by *i-V* polarization curves and EIS measurements. During the electrochemical performance test, the SFM-SDC cathode is exposed to a steam containing 74%H_2O-26% H_2, while Ru-infiltrated SFM-SDC anode is exposed to a methane atmosphere containing 5.8%CH_4-91.2%N_2-3%H_2O. Figure 4A shows the electrolysis current densities measured from OCV to 1.0 V at 750, 800 and 850 °C, respectively. At zero current, single cell with Ru-SFM-SDC anode has an OCV of -0.015, -0.0036, -0.012 V at 750, 800 and 850 °C, respectively, which are all much lower than 0.940 V for the conventional electrolysis mode in which the anode is exposed to air, indicating that a significantly lower applied cell voltage is required to produce the same amount of hydrogen in the cathode, and the high-cost electricity required can be compensated by the low-grade heat. For example, at an electrolysis current density of -0.10 A cm^{-2}, the applied electrolysis voltage required is 1.0 V for the conventional electrolysis mode with exposing the anode to air (Figure S2), while the cell voltage is significantly decreased to 0.046 V when the anode is exposed to methane in the methane-assisted electrolysis process. On the other hand, it should be noted that those OCV values are still higher than the theoretical value of -0.063, -0.084 and -0.109 V, which is strongly affected by the operating conditions, such as the operating temperature, inlet gas composition, and catalytic activities of the anode, implying that the catalytic properties of the Ru-SFM-SDC anode with a Ru loading of 1.5 wt.% are not enough for efficient POM reaction, and further work, such as more Ru loading and other advanced catalysts need to be done to further accelerate the kinetics of POM reaction in order to further lower the OCV of the cells and reduce the electricity consumption. However, the discrepancy between the OCV and Nernst potential is lower than that of SFM-SDC (Figure S2) and Pd-C-CeO_2-YSZ electrode[26], indicating that the catalytic activity of SFM-SDC composite anode has been effectively enhanced by infiltrating Ru catalysts. Moreover, the significantly lowered OCV demonstrates that the electrical energy consumed for water splitting has been remarkably reduced by introducing the reducing gas of CH_4 because OCV represents the minimum cell voltage required to pump the oxygen ions across the electrolyte.

Figure 4B represents the CH_4 conversion, CO selectivity and H_2 selectivity in the anode side of the electrolyzer recorded at 850 °C as a function of the applied cell voltage when the electrolyzer is operated in POM assisted electrolysis mode. It can be seen that when the cell is operated at 850 °C under the OCV condition, CO selectivity of 79.3% and H_2 selectivity of 83.7% are achieved, while the CH_4 conversion is determined to be 32.2%, which is possibly caused by the limited electrode size as well as the SMR process. With the increase of the applied cell voltage, the electrolysis current density increases, resulting in an increased amount of the oxygen ions split from the steam in the cathode side and transported through the electrolyte because the electrolysis current density is proportional to the amount of transported oxygen ions based on the Faraday equation, providing a great potential to further partially oxidize methane to syngas. Unfortunately, it can be seen from Figure 4B that with increasing the applied cell voltage, both the CO selectivity and H_2 selectivity gradually decrease. As the applied cell voltage increases from OCV to OCV+0.15 V, the CO selectivity and H_2 selectivity are gradually decreased from 79.3% and 83.7% to 66.4% and 69.6%, respectively, and further decreased to 30.9% and 40.0% when a voltage of OCV+0.45 V is applied on the

electrolyzer. These relatively lower CH_4 conversion rate and CO selectivity might be attributed to the difference between the gaseous oxygen and oxygen species formed on electrode catalysts[33-35]. These results imply that the pumped oxygen ions may first react with CO and H_2 to form CO_2 and H_2O instead of the expected POM reaction to syngas. Therefore, the anode composition as well as operating conditions need to be further improved to simultaneously increase the selectivity of H_2 and CO as well as the CH_4 conversion.

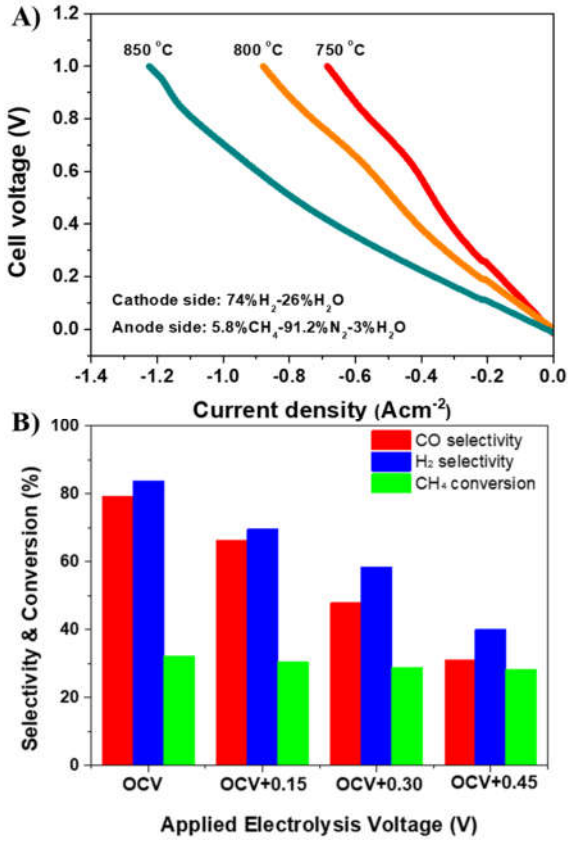

Figure 4 A) *i-V* curves of Ru infiltrated electrolyzer for POM assisted steam electrolysis measured at 750-850 °C, and B) CH_4 conversion, CO selectivity and H_2 selectivity in the anode of the electrolyzer operated in POM assisted mode at 850 °C. During the operation, the anode and the cathode are exposed to 5.8%CH_4-91.2%N_2-3%H_2O and 74%H_2-26%H_2O atmosphere, respectively.

Electrochemical impedance spectra (EIS) under OCV condition at 750, 800, and 850 °C are also measured to investigate the electrochemical performance of Ru infiltrated SFM-SDC electrode for POM assisted steam electrolysis. Figure 5A shows the Nyquist plot of the impedance spectra measured under the OCV condition at 750, 800 and 850 °C, respectively. In the Nyquist plot, high-frequency intercept and low-frequency intercept with the *x*-axis correspond to the ohmic resistance (R_{ohmic}) and total cell resistance (R_{total}), respectively, while the difference between these two intercepts represents the electrode polarization resistance (R_p). As summarized in Table 1, the R_{ohmic} values are measured to be 0.51, 0.36, and 0.28 Ω cm^2 at 750, 800, and 850 °C, respectively, while the corresponding R_{total} values are 1.44, 0.88, and 0.66 Ω cm^2, respectively. Therefore, the R_p values are calculated to be 0.93, 0.52, and 0.38 Ω cm^2 at 750, 800, and 850 °C, respectively. These results demonstrate that the resistances including R_{ohmic}, R_{total} and R_p decrease remarkably with increasing the operating temperature, which can be explained by the increased oxygen ionic conductivity of the electrolyte and improved electrocatalytic activity of the electrodes at elevated temperatures. The electrode polarization resistances for the electrolyzer with Ru-SFM-SDC electrode are also compared with those for the electrolyzers with bare SFM-SDC electrode and Ni infiltrated SFM-SDC electrode. It can be found that the electrode polarization resistance of the cells with Ru infiltrated SFM-SDC electrode is much lower than those with bare SFM-SDC electrode at the entire temperature range of 750-850 °C, and also lower than those for the cells with the introduction of 3.9 wt% Ni nanoparticles. For example, at 850 °C, an electrode polarization resistance of 0.52 Ω cm^2 is obtained for the bare SFM-SDC electrolyzer. When 3.9 wt% Ni nanoparticles are infiltrated into the SFM-SDC anode skeleton, the electrode polarization resistance is reduced to 0.46 Ω cm^2, and the electrode polarization resistance further reduces to 0.38 Ω cm^2 after the impregnation of 1.5 wt.% Ru nanoparticles. Since the materials and the thickness of each component of the cells are identical, the differences of the electrode polarization resistance of the cells come from the introduction of advanced nano-catalysts in the anode. More importantly, it can be seen from Fig. S3 that CH_4 conversion, CO selectivity and H_2 selectivity in the anode of the electrolyzers have been effectively enhanced after the introduction of Ru catalysts into bare SFM-SDC anode when the electrolyzer is operated in POM assisted mode at 850 °C and OCV condition, further confirming the superiority of SFM-SDC anode infiltrated with Ru catalyst. These results demonstrate that the catalytic properties of the anode for methane oxidation are effectively enhanced by introducing Ru nano-catalysts into the SFM-SDC anode skeleton.

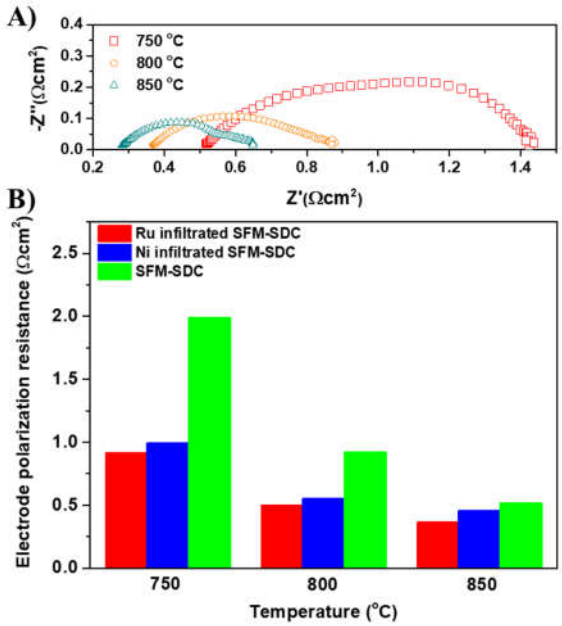

Figure 5 A) Impedance spectra of cells with Ru infiltrated anode for POM assisted steam electrolysis recorded under the OCV condition at 750-850 °C, and B) Comparison of electrode polarization resistances measured at 750-850 °C with SFM-SDC and Ni infiltrated SFM-SDC anode. During the operation, the anode and the cathode are exposed to 5.8%CH_4-91.2%N_2-3%H_2O and 74%H_2-26%H_2O atmosphere, respectively.

Table 1 The R_{ohmic}, R_{total}, and R_p values (Ω cm²) obtained from the impedance spectra of the Ru infiltrated electrolyzer measured at 750-850 °C under OCV condition

Temperature	750	800	850
R_{ohmic}	0.51	0.36	0.28
R_p	0.93	0.52	0.38
R_{total}	1.44	0.88	0.66

3.3 Long-term stability properties

The durability of the electrolyzer for POM assisted steam electrolysis process has also been examined under a constant electrolysis current density of -0.17 Acm^{-2}. As shown in Figure 6A, there is no observable degradation in a 31 h test, and a very impressive stable cell performance is achieved when the electrolyzer is operated under POM assisted steam electrolysis condition, which could be ascribed to the excellent sintering and coking resistances[47]. The sintering resistance of Ru-SFM-SDC anode could be explained by the good sintering resistance of Ru nanoparticles and SFM-SDC composite oxide, while the coking resistance could be confirmed by unobservable peaks for C-C bonds (D bond and G bond) examined for the post-test sample using Raman spectroscopy technique (Figure 6B)[48-50]. Additionally, the average size of Ru particles before and after durability test is calculated to be 96 and 95 nm from Fig. 2C and Fig. 6C, respectively, demonstrating that no obvious particle coarsening occurs during the operation. The result indicates that Ru nanoparticles have high sintering resistance at 850 °C due to its high melting point and isolating distribution[51,52].

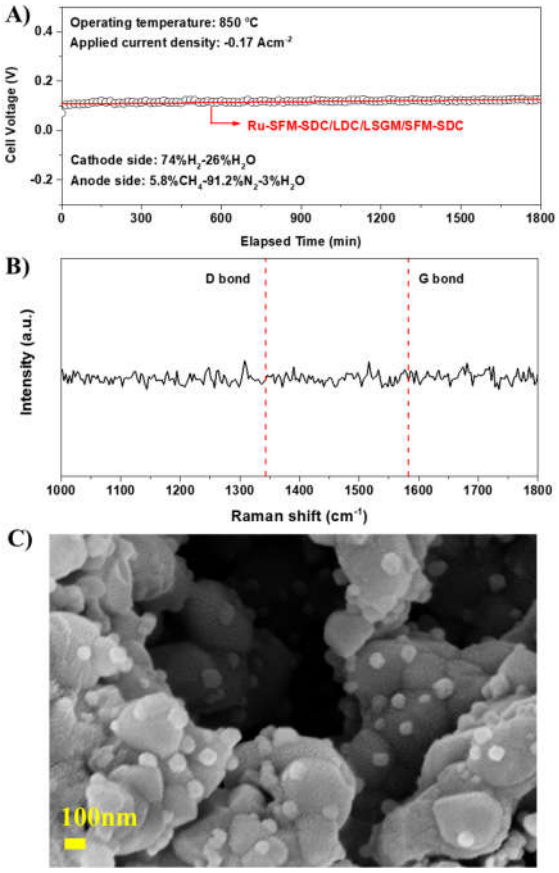

Figure 6 A) Durability of Ru infiltrated single cell for methane assisted steam electrolysis process at 850 °C and an electrolysis current density of -0.17 Acm^{-2}, B) Raman spectrum, and C) SEM image of the post-test Ru infiltrated SFM-SDC electrode.

i-V curves and EIS before and after 31-hours test are also recorded under OCV condition at 850 °C to further investigate the stability of the Ru infiltrated electrolyzer, and the results are presented in Figure 7. Figure 7A compares the *i-V* curves, and it is shown that the two curves are negligibly changed at low current density (0~-0.4 Acm^{-2}) or low cell voltage (OCV~ 0.25V), while the electrochemical performance are enhanced at high current density, especially when the current density is higher than -0.8 Acm^{-2} or the applied cell voltage is larger than 0.4 V. For example, at a cell voltage of 0.6V, the electrolysis current density is accelerated from -0.90 to -1.06 Acm^{-2}, meanwhile, at an electrolysis current density of -1.0 Acm^{-2}, the applied cell voltage required is decreased from 0.71 to 0.56 V. These results are also confirmed by the decreased total resistance of the electrolyzer as well as the electrode polarization resistance (Figure 7B). It is also found that the ohmic resistance is almost stable after testing, but the total resistance is observably decreased from 0.66 to 0.62 Ωcm², indicating that the electrode polarization resistance is decreased and the electrode process is slightly activated during the durability testing. In addition, imaginary part of the Bode plot in the EIS is also utilized to study the electrochemical activation process, and it can be seen from Figure 7C that the resistances located at the frequency range of

0.5 to 100 Hz are effectively decreased after the durability testing, demonstrating that the electrolyzer has been effectively activated by operating at a constant electrolysis current density of -0.17 Acm^{-2} for 31 hours. As it has been well known that the electrode polarization resistance is strongly affected by several factors, such as gas diffusion in the anode, adsorption, surface diffusion, and charge transfer. To better identify the mechanism for the enhancement of the Ru-SFM-SDC electrode operated in POM assisted steam electrolysis process, distribution relaxation of time (DRT) analysis, a newly developed tool for analyzing electrochemical impedance spectra[53-60], has been applied to further analyze the impedance spectra. Figure 7D presents the DRT analysis results of the EIS data in Figure 7B. It can be found in Figure 7D that each spectrum can be divided into 5 peaks, denoted by P1-5. According to the results reported by Hauch *et al.*[53], low-frequency P1 at 0.05-0.5 Hz is possibly ascribed to methane reforming; P2 located at 1-10 Hz is strongly associated with gas conversion in the electrodes; and P3 in the middle frequency range of 10-100 Hz is affected by gas diffusion in the electrodes, while the other high-frequency peaks (P4 and P5) are probably attributed to cathode and anode electrochemical reactions, such as surface diffusion, charge transfer, respectively. After the durability testing, all the peaks decrease except P1, indicating that the electrode reaction process is effectively accelerated, while the methane reforming process presented by P1 is stable. These results demonstrate that the electrolyzer with Ru-SFM-SDC electrode is effectively activated, and no degradation is induced during the durability testing.

Consequently, it is concluded that introduction of stable Ru catalyst into SFM-SDC anode via the ion-impregnation method can effectively accelerate the anode reaction process by enlarging the TPBs and increasing the catalytic activity, and thus strongly enhance electrochemical performance of the electrolyzer operated in POM assisted mode. Meanwhile, Ru catalyst nanoparticles can benefit POM reaction, and simultaneously increase the CH_4 conversion and H_2/CO selectivity. In addition, no degradation but a little improvement in electrochemical performance has been observed during the operation. These results indicate that the Ru-SFM-SDC electrode is a very promising anode for POM assisted steam electrolysis application due to the impressive electrochemical performance and good stability during the operation.

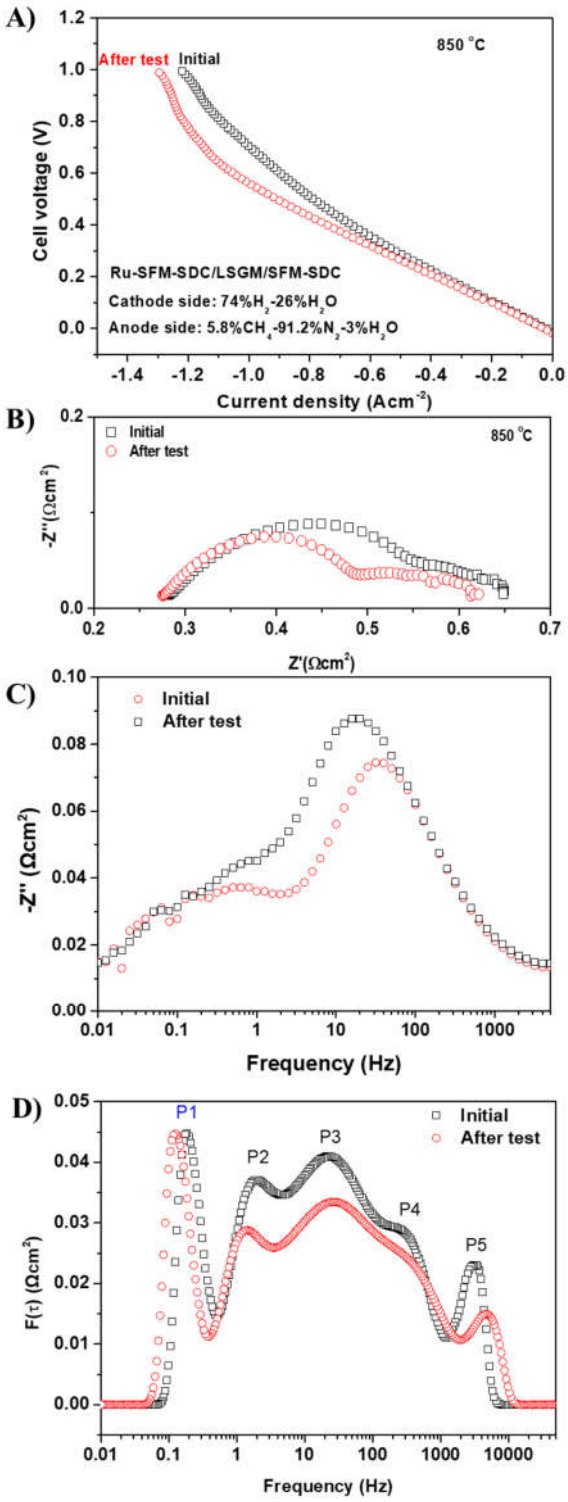

Figure 7 A) *i-V* curves, B) electrochemical impedance spectra, C) Bode plot of the imaginary part of the impedance spectra, and D) DRT analysis results of Ru infiltrated electrolyzer for POM assisted steam electrolysis before and after test measured at 850 °C under the OCV condition.

4. Conclusions

In this work, we present a novel concept of POM assisted steam electrolysis process to simultaneously produce syngas and hydrogen in the anode and cathode, respectively. In such process, certain amount of expensive electrical energy could be compensated by the use of low grade thermal energy from external heat sources. The conceptual process has been demonstrated in a Ru-SFM-SDC electrolyzer, and OCV is significantly decreased from 0.940 to -0.012 V at 850 °C when the anode and cathode are exposed to 5.8%CH_4-91.2%N_2-3%H_2O and 74%H_2O-26% H_2, respectively, which is very close to the theoretical Nernst value (-0.102 V). Experimental results reveal that Ru-SFM-SDC anode is a promising candidate anode for POM assisted steam electrolysis application because of its impressive electrochemical performance and good stability during the operation. At 0.6 V and 850 °C, the electrolysis current density of -1.06 Acm^{-2} is obtained for the electrolyzer with Ru-SFM-SDC anode, which is much higher than that (-0.54 Acm^{-2}) for the electrolyzer with bare SFM-SDC anode. Furthermore, the electrode polarization resistance at OCV condition and 850 °C is significantly decreased from 0.516 to 0.367 Ωcm^2. A long-term 31-hour durability testing reveals a slight enhancement of the cell performance due to activation of the electrode as confirmed by *i-V* curves, EIS and DRT results.

Conflicts of interest

There are no conflicts to declare.

Acknowledgements

This work was supported by National Natural Science Foundation of China (51602228, 51502207, 21673062), Natural Science Foundation of Jiangsu Province of China (BK20160380), Natural Science Foundation of Hubei Province of China (2016CFB243, 2017CFB655), the China Postdoctoral Science Foundation (2016M590712, 2017T100575), National Key R&D Program of China (2017YFA0700104), and the U.S. National Science Foundation (1832809).

Notes and references

‡ Footnotes relating to the main text should appear here. These might include comments relevant to but not central to the matter under discussion, limited experimental and spectral data, and crystallographic data.

§

§§

etc.

1 G. Cipriani, V. Di Dio, F. Genduso, D. La Cascia, R. Liga, R. Miceli, G.R. Galluzzo, *Int. J. Hydrogen Energ.*, 2014, **39**, 8482-8494.
2 K. Mazloomi, C. Gomes, *Renew. Sust. Energ. Rev.*, 2012, **16**, 3024-3033.
3 S.E. Hosseini, M.A. Wahid, *Renew. Sust. Energ. Rev.*, 2016, **57**, 850-866.
4 A. Züttel, A. Remhof, A. Borgschulte, O. Friedrichs, *Philos. T. R. Soc. A*, 2010, **368**, 3329-3342.
5 A. Haryanto, S. Fernando, N. Murali, S. Adhikari, *Energ. Fuel.*, 2005, **19**, 2098-2106.
6 A.P. Simpson, A.E. Lutz, *Int. J. Hydrogen Energ.*, 2007, **32**, 4811-4820.
7 T.L. LeValley, A.R. Richard, M. Fan, *Int. J. Hydrogen Energ.*, 2014, **39**, 16983-17000.
8 L. Bi, S. Boulfrad, E. Traversa, *Chem. Soc. Rev.*, 2014, **43**, 8255-8270.
9 M. Ni, M.K. Leung, D.Y. Leung, *Int. J. Hydrogen Energ.*, 2008, **33**, 2337-2354.
10 T. Liu, Y. Wang, Y. Zhang, S. Fang, L. Lei, C. Ren, F. Chen, *Electrochem. Commun.*, 2015, **61**, 106-109.
11 Y. Zheng, J. Wang, B. Yu, W. Zhang, J. Chen, J. Qiao, J. Zhang, *Chem. Soc. Rev.*, 2017, **46**, 1427-1463.
12 Y. Wang, T. Liu, L. Lei, F. Chen, *Fuel Process. Technol.*, 2017, **161**, 248-258.
13 M. Laguna-Bercero, *J. Power sources*, 2012, **203**, 4-16.
14 S.D. Ebbesen, S.H. Jensen, A. Hauch, M.B. Mogensen, *Chem. Rev.*, 2014, **114**, 10697-10734.
15 Y. Wang, T. Liu, M. Li, C. Xia, B. Zhou, F. Chen, *J. Mater. Chem. A*, 2016, **4**, 14163-14169.
16 Y. Wang, X. Lei, Y. Zhang, F. Chen, T. Liu, *J. Power sources*, 2018, **405**, 114-123.
17 Y. Wang, J. Xu, X. Meng, T. Liu, F. Chen, *Electrochem. Commun.*, 2017, **79**, 63-67.
18 J. Lin, L. Chen, T. Liu, C. Xia, C. Chen, Z. Zhan, *J. Power sources*, 2018, **374**, 175-180.
19 Y. Wang, T. Liu, L. Lei, F. Chen, *J. Power sources*, 2017, **344**, 119-127.
20 G. Cinti, G. Bidini, K. Hemmes, *Int. J. Hydrogen Energ.*, 2016, **41**, 11857-11867.
21 L. Lei, Y. Wang, S. Fang, C. Ren, T. Liu, F. Chen, *Appl. Energ.*, 2016, **173**, 52-58.
22 J. Lu, C. Zhu, C. Pan, W. Lin, J.P. Lemmon, F. Chen, C. Li, K. Xie, *Sci. Adv.*, 2018, **4**, eaar5100.
23 W. Wang, R.J. Gorte, J.M. Vohs, *Chem. Eng. Sci.*, 2008, **63**, 765-769.
24 Y. Patcharavorachot, S. Thongdee, D. Saebea, S. Authayanun, A. Arpornwichanop, *Energ. Convers. Manage.*, 2016, **120**, 274-286.
25 J. Martinez-Frias, *Int. J. Hydrogen Energ.*, 2003, **28**, 483-490.
26 W. Wang, J.M. Vohs, R.J. Gorte, *Top. Catal.*, 2007, **46**, 380-385.
27 N. Visitdumrongkul, P. Tippawan, S. Authayanun, S. Assabumrungrat, A. Arpornwichanop, *Energ. Convers. Manage.*, 2016, **129**, 189-199.
28 B.C. Enger, R. Lødeng, A. Holmen, *Appl. Catal. A-Gen.*, 2008, **346**, 1-27.
29 A.P. York, T. Xiao, M.L. Green, *Top. Catal.*, 2003, **22**, 345-358.
30 H.E. Figen, S.Z. Baykara, *Int. J. Hydrogen Energ.*, 2015, **40**, 7439-7451.
31 A. Scarabello, D. Dalle Nogare, P. Canu, R. Lanza, *Appl. Catal. B-Environ.*, 2015, **174**, 308-322.
32 R.K. Singha, A. Shukla, A. Yadav, L.S. Konathala, R. Bal, *Appl. Catal. B-Environ.*, 2017, **202**, 473-488.
33 B. Hua, N. Yan, M. Li, Y.-q. Zhang, Y.-f. Sun, J. Li, T. Etsell, P. Sarkar, K. Chuang, J.-L, Luo, *Energy Environ, Sci.*, 2016, **9(1)**, 207-215.
34 B. Hua, N. Yan, M. Li, Y.-F. Sun, Y.-Q. Zhang, J. Li, T. Etsell, P. Sarkar, J.-L. Luo, *Adv. Mater.*, 2016, **28(40)**, 8922-8926.
35 Y.-F. Sun, Y.-Y. Wu, Y.-Q. Zhang, J.-H. Li, Y.-X. Shi, B. Hua, J.-L. Luo, *Chem. Commun.*, 2016, **52(94)**, 13687-13690.
36 J.A. Velasco, C. Fernandez, L. Lopez, S. Cabrera, M. Boutonnet, S. Järås, *Fuel*, 2015, **153**, 192-201.
37 H.E. Figen, S.Z. Baykara, *Int. J. Hydrogen Energ.*, 2018, **43**, 1129-1138.
38 S. Das, R. Gupta, A. Kumar, M. Shah, M. Sengupta, S. Bhandari, A. Bordoloi, *ACS Appl. Nano Mater.*, 2018, **1**, 2953-2961.

39 M. Li, B. Hua, Y. Zeng, B. S. Amirkhiz, J.-L. Luo, *J. Mater. Chem. A*, 2018, **6(31)**, 15377-15385.
40 Y. Xue, J. T. S. Irvine, *J. Mater. Chem. A*, 2017, **5(15)**, 7081-7090.
41 X. Zhang, L. Liu, Z. Zhao, B. Tu, D. Ou, D. Cui, X. Wei, X. Chen, M. Cheng, *Nano Lett*., 2015, **15(3)**, 1703–1709.
42 K. J. Yoon, M. Biswas, H.-J. Kim, M. Park, J. Hong, H. Kim, J.-W. Son, J.-H. Lee, B.-K. Kim, H.-W. Lee, *Nano Energy*, 2017, **36**, 9-20
43 Q. Liu, X. Dong, G. Xiao, F. Zhao, F. Chen, *Adv. Mater.*, 2010, **22**, 5478-5482.
44 A. Mineshige, T. Taji, Y. Muroi, M. Kobune, S. Fujii, N. Nishi, M. Inaba, Z. Ogumi, *Solid State Ionics*, 2000, **135**, 481-485.
45 A. Korotcov, H.P. Hsu, Y.S. Huang, P.C. Liao, D.S. Tsai, K.K. Tiong, *J. Alloy. Compd.*, 2007, **442**, 310-312.
46 C. Liu, K.S. Kim, J. Baek, Y. Cho, S. Han, S.-W. Kim, N.-K. Min, Y. Choi, J.-U. Kim, C.J. Lee, *Carbon*, 2009, **47**, 1158-1164.
47 Y. Li, B. Hu, C. Xia, W.Q. Xu, J.P. Lemmon, F. Chen, *J. Mater. Chem. A*, 2017, **5**, 20833-20842.
48 T. Liu, X. Chen, J. Wu, Z. Sheng, G. Liu, Y. Wang, *J. Electrochem. Soc.*, 2017, **164**, F1130-F1135.
49 K.S. Blinn, H. Abernathy, X. Li, M. Liu, L.A. Bottomley, M. Liu, *Energ. Environ. Sci.*, 2012, **5**, 7913-7917.
50 H. S. Whang, M. S. Choi, J. Lim, C. Kim, I. Heo, T.-S. Chang, H. Lee, *Catal. Today.*, 2017, **293-294**, 122-128.
51 D. Li, R. Li, M. Lu, X. Lin, Y. Zhan, L, Jiang, *Appl. Catal.-B Environ.*, 2017, **200**, 566-577.
52 A. Hauch, A. Hagen, J. Hjelm, T. Ramos, *J. Electrochem. Soc.*, 2014, **161**, F734-F743.
53 Y. Zhang, Y. Chen, M. Yan, F. Chen, *J. Power sources*, 2015, **283**, 464-477.
54 M. Saccoccio, T.H. Wan, C. Chen, F. Ciucci, *Electrochim. Acta*, 2014, **147**, 470-482.
55 T.H. Wan, M. Saccoccio, C. Chen, F. Ciucci, *Electrochim. Acta*, 2015, **184**, 483-499.
56 Y. Zhang, Y. Chen, M. Li, M. Yan, M. Ni, C. Xia, *J. Power sources*, 2016, **308**, 1-6.
57 N. Shi, F. Su, D. Huan, Y. Xie, J. Lin, W. Tan, R. Peng, C. Xia, C. Chen, Y. Lu, *J. Mater. Chem. A*, 2017, **5**, 19664-19671.
58 Y. Chen, Y. Choi, S. Yoo, Y. Ding, R. Yan, K. Pei, C. Qu, L. Zhang, I. Chang, B. Zhao, Y. Zhang, H. Chen, Y. Chen, C. Yang, B. deGlee, R. Murphy, J. Liu, M. Liu, *Joule*, 2018, **2**, 938-949.
59 X. Chen, J. Lin, L. Sun, T. Liu, J. Wu, Z. Sheng, Y. Wang, Electrochim. Acta, 2019, 298, 112-120.
60 M. Zheng, S. Wang, Y. Yang, C. Xia, *J. Mater. Chem. A*, 2018, **6**, 2721-2729.